Numerical simulation of Contact Acoustic Nonlinearities in damaged CFRP laminates through laser-induced guided waves

Shain Azadi[1][0000-0002-8938-9598] and Valter Carvelli[1][0000-0001-5272-608X]

[1] Department A.B.C., Politecnico di Milano, Milan, Italy
shain.azadi@polimi.it

Abstract. The importance of Carbon Fiber Reinforced Polymer (CFRP) materials in numerous industries demands more accurate and timely damage identification methods. Delamination, a typical damage mechanism, heavily affects laminates' performance and requires prompt detection to ensure the safeness and operability of CFRP structures. This paper explores the use of guided waves to excite contact acoustic nonlinearities (CANs) in a damaged quasi-isotropic CFRP laminate. Delamination-induced CANs are exploited to identify the shape and position of delamination. The Finite Element Method (FEM) is used to model CAN generation and propagation. In the numerical model, a Gaussian laser beam heating the laminate surface induces Ultrasonic Guided Wave (UGW) propagation. The vertical displacement of the damaged laminate is measured by simulating a Scanning Laser Doppler Vibrometer (SLDV). Using 2D Continuous Wavelet Transformation (2D-CWT), the 2D wavefield is converted into the spatiotemporal frequency domain and analyzed to detect resonance frequencies. Two case scenarios are analyzed for a 16 plies CFRP laminate: delamination between the 13th and 14th layer (near the surface) and delamination between the 4th and 5th layer (near the bottom). The ability of this method to detect and assess both shallow and deep delamination in CFRP laminates is confirmed.

Keywords: Guided waves, Composite Laminates, Damage, Finite Element Modelling.

1 Introduction

Carbon Fiber Reinforced Polymer (CFRP) laminates have found extensive application as structural materials in various engineering sectors (e.g., aerospace, renewable energy, and civil engineering), thanks to their high strength-to-weight and stiffness-to-weight ratios, resilience, and chemical inertness [1, 2]. However, CFRP structures are susceptible to degradation caused by manufacturing anomalies, extreme operational conditions, impacts, and fatigue [3–5]. Undetected damage onset can lead to rapid

compromise of structural integrity and functionality of CFRP structures, risking premature failure.

Among typical damage modes, delamination indicates the detachment of layers within the laminate structure, resulting in internal voids or gaps [6]. Delamination can reduce the load-carrying capacity and stiffness of the laminate, introduces local stress concentrations [7], and, if undetected, propagate and lower resistance to impacts [8]. Closed-gap delamination is particularly complex to identify using standard methods because, under low excitations, the laminate behaves similarly to an intact material. Hence, developing efficient visualization methods to highlight this type of damage is crucial for CFRP laminates' safeness.

Non-Destructive Evaluation (NDE) methods are predominant for inspecting composite structures [9]. Among them, Ultrasonic Guided Waves (UGWs) are extensively used for structural health monitoring (SHM) [10] due to their damage sensitivity, tunable excitation wavelength, and volume coverage, which allows for the monitoring of internal regions of laminates. In recent years, Nd:YAG (neodymium-doped yttrium aluminum garnet) lasers have been used to remotely excite UGW propagation by inducing a quick local thermal expansion and contraction of the laminate [11]. Laser-induced Ultrasonic Guided Waves (LUGWs) are suitable for non-contact SHM because of the small laser footprint, which enables them to reach remote and intricately shaped parts [12]. Further, LUGWs reduce distortions related to sensor deterioration and failure, which can ultimately lead to incorrect signal recording and evaluation. When UGWs interact with delamination, the repeated contact between the two excited interfaces can generate nonlinear effects, providing insight into damage detection and diagnosis. These nonlinear effects, known as Contact Acoustic Nonlinearities (CANs) [13], determine signal distortions, such as local defect resonance [14] and harmonic generation [15], that correlate with the presence, shape, and severity of the damage.

In this paper, the delamination-induced nonlinear acoustic phenomena are predicted using numerical simulations. The estimated finite element vertical displacement field visualizes the 2D wavefield highlighting the wave-delamination interaction in a quasi-isotropic CFRP laminate. The frequencies generated by CANs are observed in the spatiotemporal-frequency domain for different depths of the delamination.

2 Numerical Model Features

2.1 Geometry and material properties

The modeled composite, illustrated in Fig. 1, is a 16-layer CFRP quasi-isotropic laminate with stacking sequence $[(+0/+45/+90/-45)_2]_s$.

In the Finite Element Method (FEM) model, each ply is assumed to be a homogeneous mechanical equivalent elastic material. According to manufacturer specifications (Toray T7000SC/2500), the components of the anisotropic stiffness matrix and the thermal properties of the 0° ply are listed in Table 1 and 2, respectively.

The laminate plate is 100 mm long and wide and has a density ρ=1530 kg/m^3. Ply thickness is 0.14 mm, for a total thickness of 2.24 mm.

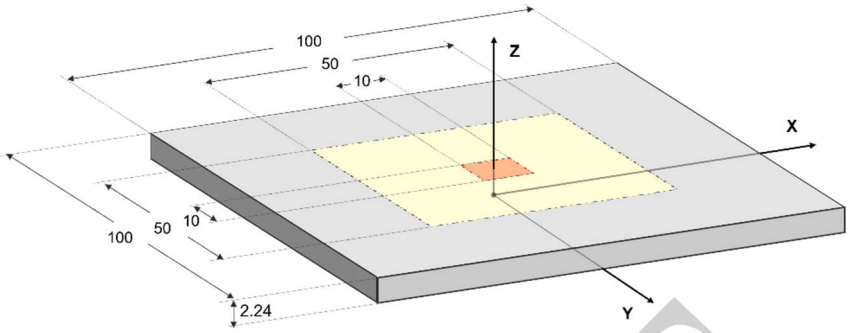

Fig. 1. Dimension of the simulated quasi-isotropic CFRP laminate with interlaminar delamination (units: mm).

A scanning window, from which the displacement field is recorded, is set from -25 mm to +25 mm (length 50 mm) along the X-axis and from -25 mm to +25 mm (width 50 mm) along the Y-axis (see Fig. 1).

The damage is a square delamination of side 10 mm located at the center of the plate. The first model has the delamination between the 13th and 14th layers (Z=1.96 mm) to simulate damage close to the top surface of the plate. In the second model, delamination is between the 4th and 5th layers (Z=0.56 mm) to evaluate an opposite scenario where the damage is far from the scanned top surface.

The dispersive properties of the composite plate can be predicted knowing the anisotropic stiffness matrix, the density, and the thickness of the unidirectional lamina, the stacking sequence, and the wave propagation direction. A comparison between exact (e.g., Global Matrix Method (GMM) [16]) and approximated (e.g., Semi-Analytical Finite Element Method [17]) methods to calculate the dispersion curves [18] highlights that, for low *fd* values (<1 MHz·mm), the Fifth-Order Shear Deformation Theory (5-SDT) [19] provides the best accuracy-computational time trade-off. Thus, 5-SDT is used to calculate the frequency-wavenumber plots for a 0° wave propagation direction (see Fig. 2).

Table 1. Stiffness matrix components of the homogenized CFRP unidirectional ply with 0° fiber orientation (T700SC/2500).

Elastic Stiffness Constants	Value
C_{11}	133.090 GPa
C_{12}	4.978 GPa
C_{13}	4.978 GPa
C_{22}	10.714 GPa
C_{23}	5.345 GPa
C_{33}	10.714 GPa
C_{55}	4.800 GPa

Table 2. Thermal parameters of the homogenized CFRP unidirectional ply with 0° fiber orientation (T700SC/2500).

Parameter	Value	Definition
$\{k_1, k_2, k_3\}$	{60, 0.59, 0.59} W/(m·K)	Thermal conductivity (X, Y, and Z)
C_p	923 J/(kg·K)	Heat capacity at constant pressure
$\{\alpha_1, \alpha_2, \alpha_3\}$	{4.8e-7, 4.0e-5, 4.0e-5} 1/K	Coefficient of thermal expansion (X, Y, and Z)

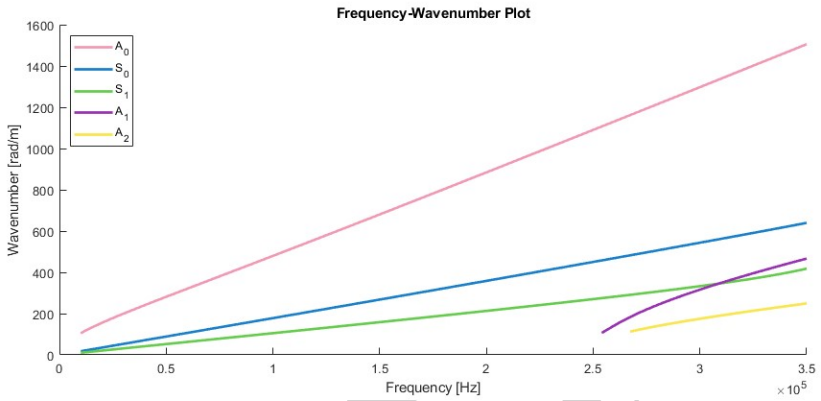

Fig. 2. Frequency-Wavenumber plot of CFRP quasi-isotropic laminate $[(+0/+45/+90/-45)_2]_s$ by Fifth-Order Shear Deformation Theory for a 0° propagating UGW.

2.2 Numerical modeling

LUGW propagation in a damaged CFRP laminate is simulated through thermo-mechanical coupling using COMSOL Multiphysics software.
Computing wave propagation in media through dynamic explicit analysis requires strict temporal and spatial resolution. The spatial resolution of the numerical model, namely the finite element dimension, allows for the correct estimation only of wavelengths up to twice the mesh dimension and best practice suggests scaling up this ratio 10-20 times [20]. Similarly, temporal resolution follows the Nyquist-Shannon theorem, setting the maximum recordable frequency at half of the sampling one.

In this study, the frequency used for calculating the spatial resolution is 350 kHz, which allows for a suitable approximation of frequencies up to 1 MHz. Thus, according to the frequency-wavenumber plot in Fig. 2, the angular wavenumber of the fundamental symmetric mode S_0 (k_{S_0}) is about 639 rad/m or 102 m^{-1}, and the angular wavenumber of the fundamental antisymmetric mode A_0 (k_{A_0}) is about 1505 rad/m or 239 m^{-1}. Consequently, to fully solve fundamental wave modes propagation in the laminate, solid hexahedral mesh elements are adopted with maximum dimension d according to Eq. (1).

$$d = \min\left(\frac{1}{k_{S_0}\cdot 10}, \frac{1}{k_{A_0}\cdot 10}\right) \tag{1}$$

The model boundary conditions are supposed to reproduce soft unilateral supports at the corners by using spring-like elements. To isolate the effects of wave-damage interaction, a low-reflective boundary condition is applied to the plate's outer edges.

The wave-delamination behavior is governed by a pressure-gap relation [21, 22]. Interlaminar delamination is implemented using a thin elastic layer boundary condition. This condition first decouples the displacements between the two sides of the boundary and then connects them using equal forces per unit area. These forces, proportional to the relative normal displacement, have opposite directions. The boundary forces ensure negligible penetration between the surfaces in case of contact. Their analytic formula is reported in Eq. (2).

$$N = C^2 \cdot a^2 \ (a > 0) \tag{2}$$

In Eq. (2), $C = 6e10^{\ 10}\ Pa^{\frac{1}{2}}\ m^{-1}$ is a material-dependent constant, obtained by matching the experimental relation between the contact pressure and the gap distance, and a is the normal displacement considered as an overclosure distance. Thus, contact occurs when a is positive.

LUGW propagation is excited through an Nd:YAG laser, which induces a rapid thermal expansion and contraction of the laminate's surface. The numerical model simulates laser illumination through a Gaussian Deposited Beam Power model. Laser parameters are listed in Table 3. Laser energy density is estimated, according to [11], by Eq. (3), where $f(r)$ is the laser spatial variation and $p(t)$ is the laser temporal variation.

$$I_0 = \frac{E_p}{\left(\int_0^\infty f(r) 2\pi r \, dr\right)\left(\int_0^\infty p(t) \, dt\right)} \tag{3}$$

Table 3. Nd:YAG laser properties

Parameter	Value	Definition
τ	7e-9 s	Laser pulse duration
r	5e-4 m	Laser beam radius
E_p	1.3e-4 J	Absorbed pulse energy
I_0	2.4e10 W/m^2	Laser energy density
P	1.9e4 W	Laser power output

3 Results

3.1 Wavefield analysis

To evaluate the effect of wave propagation through damaged quasi-isotropic CFRP laminates, the numerical models simulate a Scanning Laser Doppler Vibrometer (SLDV), model PSV-500 (Polytech, GmbH) [23]. The vertical displacement field is measured using a spatial resolution of 0.1 mm and a temporal resolution of 1e-7 s.

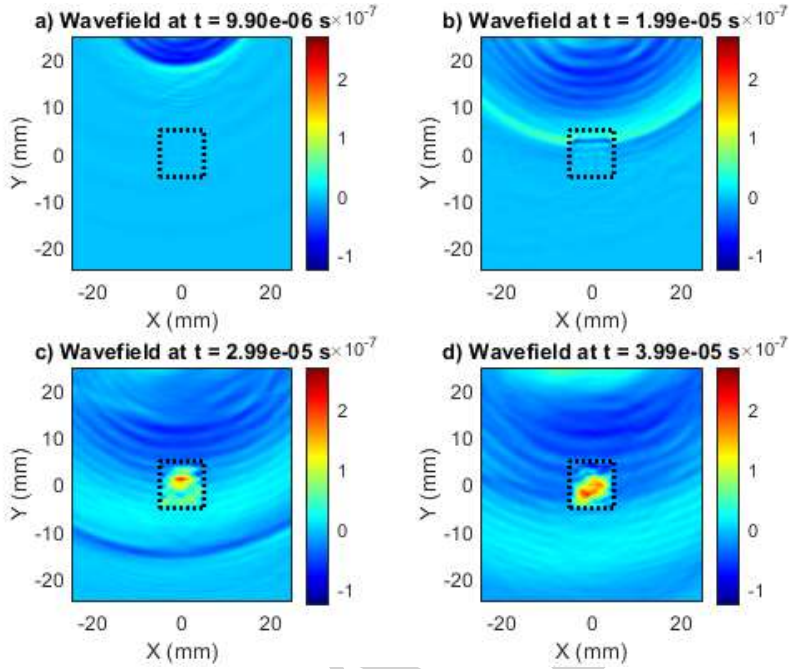

Fig. 3. Simulated vertical displacement field measured on the top surface of the CFRP laminate Z=2.24 mm (X-Y plane) with delamination (dotted square) at Z=1.96 mm. Spatial window at time (a) 10, (b) 20, (c) 30, and (c) 40 μs.

In both models, the vertical displacement field of the laminate is measured on the top of the plate inside a spatial window (50 mm x 50 mm, see Fig. 1). Wavefields are plotted in the top X-Y plane at different time instants in Fig. 3 and Fig. 4.

In Fig. 3a, the faster S_0 wave propagates through the spatial window, while the A_0 wave, having a group velocity of around 1500 m/s, reaches the initial part of the scanned area. The A_0 wave is clearly recognizable by the higher amplitude peak of the wavefront. In Fig. 3b, the A_0 wave reaches the delamination generating an abrupt distortion of the propagating wavefront. When the A_0 wave passes through the delaminated area, the repeated contacts between the two interfaces in the damaged portion generate higher amplitude components (Fig. 3c). In Fig. 3d, the contact forces induce localized amplitude peaks within the delamination area.

In Fig. 4a, like Fig. 3a, the S_0 and A_0 wavefronts propagate through the spatial window. However, in Fig. 4b, when the A_0 wave reaches the delamination, no significant alteration of the propagating wavefront is visualized. The backside delamination does not affect the wavefield, as shown in Fig. 4c and Fig. 4d.

Therefore, direct visualization of the wavefield does not provide insight into delamination location or shape when located far from the scanned surface, and further post-processing is required to acquire such information.

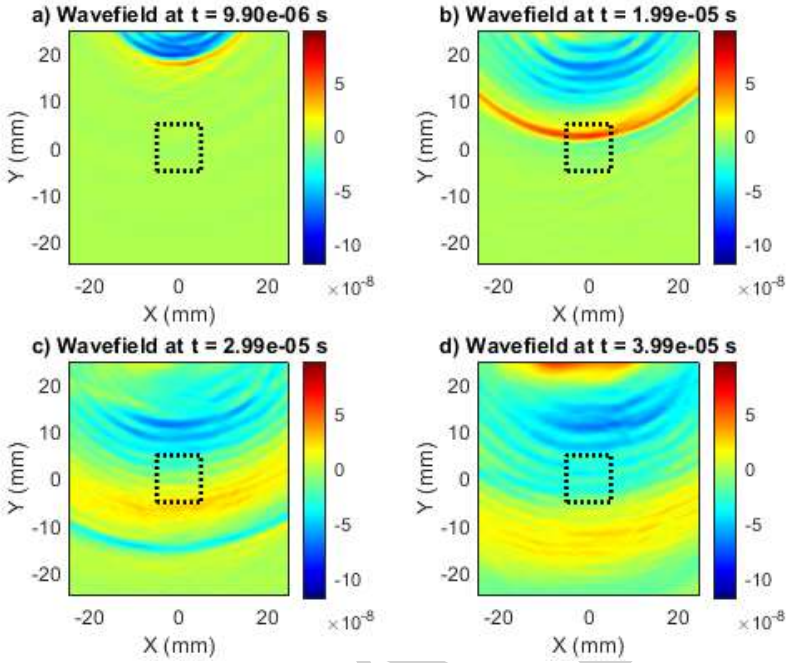

Fig. 4. Simulated vertical displacement field measured on the top surface of the CFRP laminate Z=2.24 mm (X-Y plane) with delamination (dotted square) at Z=0.56 mm. Spatial window at time (a) 10, (b) 20, (c) 30, and (c) 40 μs.

3.2 Spatiotemporal frequency visualization

To further investigate the potential of 2D-wavefield in visualizing both topside and backside delamination in CFRP laminates, data, in terms of continuous images $f(x,y)$ captured at each time step, are post-processed using 2D-Continuous Wavelet Transformation (2D-CWT)[24], detailed in Eq. (4).

$$W(a,b,\theta) = \frac{1}{|a|}\int_{-\infty}^{+\infty}\int_{-\infty}^{+\infty} f(x,y)\psi^*\left(\frac{x-b_1}{a},\frac{y-b_2}{a}\right)dxdy \quad (4)$$

In Eq. (4), $W(a,b,\theta)$ is the wavelet coefficient for the scale factor a, position vector b and orientation angle θ, $\psi^*\left(\frac{x-b_1}{a},\frac{y-b_2}{a}\right)$ is the complex conjugate of the mother wavelet.

The different frequency components, in space-time visualization (Fig. 5 and Fig. 6), exhibit specific patterns enabling the identification of delamination shape and position. In Fig. 5 and Fig. 6, only the top 5% magnitude of the frequencies is displayed to better highlight the high-intensity frequency peaks.

In Fig. 5, the spatiotemporal frequency domain at f=358 kHz shows how, in the model with delamination at Z=1.96 mm, the effect of the wave-damage interaction is clearly distinguishable in the frequency domain. A high-magnitude frequency component

focuses on the delamination area (dotted in Fig. 5) with relatively lower peaks in the surrounding parts. The spatiotemporal frequency domain at *f*=358 kHz shows no distinct frequency component in the delaminated area for the model with delamination at Z=0.56 mm (Fig. 6,). However, the selected frequency component looks altered by the presence of delamination, which filters out the components at *f*=358 kHz

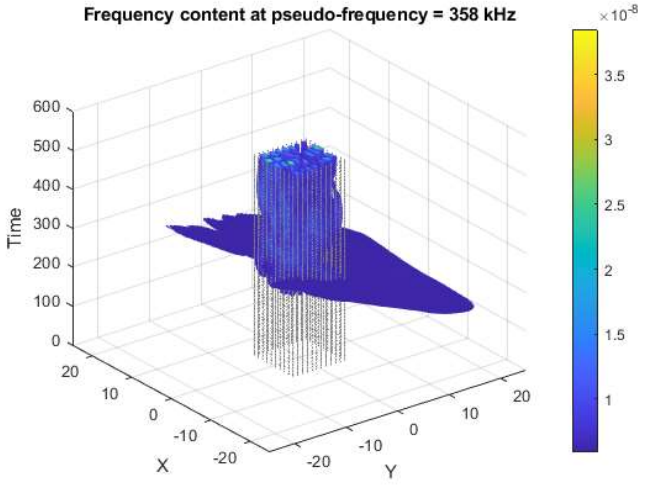

Fig. 5. Simulated spatiotemporal-frequency domain at frequency *f*=358 kHz for the quasi-isotropic CFRP laminate with centered delamination at Z=1.96 mm.

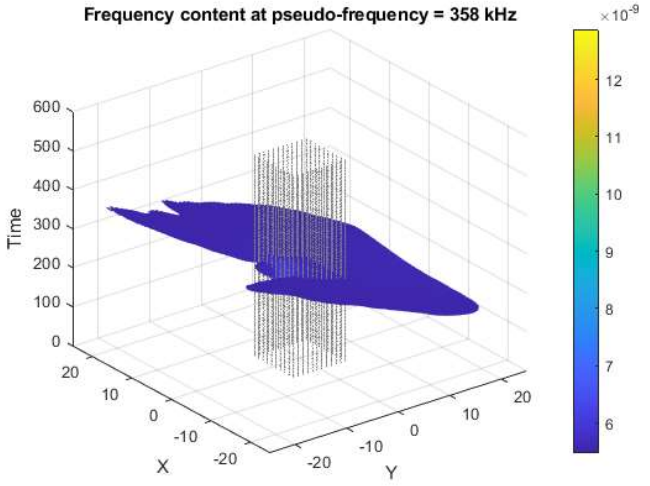

Fig. 6. Simulated spatiotemporal-frequency domain at frequency *f*=358 kHz for the quasi-isotropic CFRP laminate with centered delamination at Z=0.56 mm.

4 Conclusion

Post-processing the 2D wavefield using a spatiotemporal-frequency analysis provides further insight into the delamination of quasi-isotropic CFRP laminates and can improve its detection. Backside delamination, which is not pointed out with the vertical displacement field of the surface for this type of excitation, can also affect the frequency components throughout space and time.

In the case study of this work, the existence and location of topside delamination are visible without post-processing. Differently, the presence of backside delamination can be inferred by observing how specific frequency components are distributed in time and space.

Future research aims to improve the visualization of backside delamination by exploiting distinctive wave mode-damage interactions. Furthermore, numerical evidence will be validated through experiments.

References

1. Chung, D.D.L.: Introduction to Carbon Composites. In: Carbon Composites. pp. 88–160. Elsevier (2017)
2. Miyano, Y., Nakada, M.: Accelerated testing methodology for durability of CFRP. Compos B Eng. 191, 107977 (2020). https://doi.org/10.1016/j.compositesb.2020.107977
3. Talreja, R.: Manufacturing defects in composites and their effects on performance. In: Polymer Composites in the Aerospace Industry. pp. 99–113. Elsevier Inc. (2015)
4. Abrate, S.: Impact on Laminated Composite Materials. Appl Mech Rev. 44, 155–190 (1991). https://doi.org/10.1115/1.3119500
5. Alam, P., Mamalis, D., Robert, C., Floreani, C., Ó Brádaigh, C.M.: The fatigue of carbon fibre reinforced plastics - A review. Compos B Eng. 166, 555–579 (2019). https://doi.org/10.1016/j.compositesb.2019.02.016
6. Raju, I.S., O'Brien, T.K.: Fracture mechanics concepts, stress fields, strain energy release rates, delamination initiation and growth criteria. In: Delamination Behaviour of Composites. pp. 3–27. Elsevier (2008)
7. Bak, B.L.V., Sarrado, C., Turon, A., Costa, J.: Delamination under fatigue loads in composite laminates: A review on the observed phenomenology and computational methods. Appl Mech Rev. 66, (2014). https://doi.org/10.1115/1.4027647
8. Johnson, A.F., Toso-Pentecôte, N.: Determination of delamination damage in composites under impact loads. In: Delamination Behaviour of Composites. pp. 561–585. Elsevier (2008)
9. Gholizadeh, S.: A review of non-destructive testing methods of composite materials. Procedia Structural Integrity. 1, 50–57 (2016). https://doi.org/10.1016/j.prostr.2016.02.008
10. Mitra, M., Gopalakrishnan, S.: Guided wave based structural health monitoring: A review. Smart Mater Struct. 25, 053001 (2016). https://doi.org/10.1088/0964-1726/25/5/053001
11. Saito, O., Higuchi, N., Sen, E., Okabe, Y.: Analysis of ultrasonic waves generated by oblique incidence of a laser. Insight - Non-Destructive Testing and Condition Monitoring. 61, 714–719 (2019). https://doi.org/10.1784/insi.2019.61.12.714
12. Takatsubo, J., Wang, B., Tsuda, H., Toyama, N.: Generation Laser Scanning Method for the Visualization of Ultrasounds Propagating on a 3-D Object with an Arbitrary Shape.

Journal of Solid Mechanics and Materials Engineering. 1, 1405–1411 (2007). https://doi.org/10.1299/jmmp.1.1405

13. Solodov, I.Yu., Krohn, N., Busse, G.: CAN: an example of nonclassical acoustic nonlinearity in solids. Ultrasonics. 40, 621–625 (2002). https://doi.org/10.1016/S0041-624X(02)00186-5
14. Segers, J., Kersemans, M., Hedayatrasa, S., Calderon, J., Van Paepegem, W.: Towards in-plane local defect resonance for non-destructive testing of polymers and composites. NDT and E International. 98, 130–133 (2018). https://doi.org/10.1016/j.ndteint.2018.05.007
15. Wei, L., Chen, J.: Characterization of delamination features of orthotropic CFRP laminates using higher harmonic generation technique: Experimental and numerical studies. Compos Struct. 285, (2022). https://doi.org/10.1016/j.compstruct.2022.115239
16. Knopoff, L.: A matrix method for elastic wave problems. Bulletin of the Seismological Society of America. 54, 431–438 (1964). https://doi.org/10.1785/BSSA0540010431
17. Bartoli, I., Marzani, A., Lanza di Scalea, F., Viola, E.: Modeling wave propagation in damped waveguides of arbitrary cross-section. J Sound Vib. 295, 685–707 (2006). https://doi.org/10.1016/j.jsv.2006.01.021
18. Orta, A.H., Kersemans, M., Van Den Abeele, K.: A comparative study for calculating dispersion curves in viscoelastic multi-layered plates. Compos Struct. 294, 115779 (2022). https://doi.org/10.1016/j.compstruct.2022.115779
19. Orta, A.H., Vandendriessche, J., Kersemans, M., Van Paepegem, W., Roozen, N.B., Van Den Abeele, K.: Modeling lamb wave propagation in visco-elastic composite plates using a fifth-order plate theory. Ultrasonics. 116, 106482 (2021). https://doi.org/10.1016/j.ultras.2021.106482
20. Maio, L., Fromme, P.: On ultrasound propagation in composite laminates: advances in numerical simulation. Progress in Aerospace Sciences. 129, 100791 (2022). https://doi.org/10.1016/j.paerosci.2021.100791
21. Biwa, S., Nakajima, S., Ohno, N.: On the Acoustic Nonlinearity of Solid-Solid Contact With Pressure-Dependent Interface Stiffness. J Appl Mech. 71, 508–515 (2004). https://doi.org/10.1115/1.1767169
22. Yuan, M., Zhang, J., Song, S.-J., Kim, H.-J.: Numerical simulation of Rayleigh wave interaction with surface closed cracks under external pressure. Wave Motion. 57, 143–153 (2015). https://doi.org/10.1016/j.wavemoti.2015.03.009
23. Kudela, P., Wandowski, T., Malinowski, P., Ostachowicz, W.: Application of scanning laser Doppler vibrometry for delamination detection in composite structures. Opt Lasers Eng. 99, 46–57 (2017). https://doi.org/10.1016/j.optlaseng.2016.10.022
24. Murenzi, R.: Wavelet Transforms Associated to the n-Dimensional Euclidean Group with Dilations: Signal in More Than One Dimension. In: Combes, J.M., Grossmann, A., and Tchamitchian, P. (eds.) Wavelets. Inverse problems and theoretical imaging. pp. 239–246. Springer, Berling, Heidelberg (1990)